Progress In Electromagnetics Research, PIER 97, 417–431, 2009

TWO-PROBE EXCITED CIRCULAR RING ANTENNA FOR MIMO APPLICATION

M. Krairiksh, P. Keowsawat, C. Phongcharoenpanich and S. Kosulvit

Faculty of Engineering
King Mongkut's Institute of Technology Ladkrabang
Bangkok 10520, Thailand

Abstract—This paper presents the analysis and design of a two-probe excited circular ring antenna. The analysis is conducted by using induced emf method and transmission line model. The design process is to choose a suitable radius of the ring for a single probe antenna. Then, the suitable probe length and ring length are determined for the two-probe antenna. Finally, isolation between the two probes is enhanced by insertion of an inductor coil between the probes. The operational characteristics of the prototype antenna at the frequency of 5.2 GHz are measured and compared with calculation results. It is evident that these results are in good agreement. The antenna achieved isolation in excess of 20 dB and VSWR less than 2 : 1 over the desired bandwidth and a bidirectional radiation pattern with 4 dBi gain. This antenna is suitable for Multiple-Input Multiple-Output (MIMO) system covering a long and narrow environment.

1. INTRODUCTION

Present wireless multimedia systems require high data transmission rate. A solution for this requirement is Multiple-Input Multiple-Output (MIMO) radio systems that can transmit several parallel data streams simultaneously. It can increase the capacity of a system enormously without requiring wide spectrum. By increasing the number of antenna elements and the spacing between them, the capacity of such a system for a large angular-spread environment increases [1]. However, increasing signal correlation, as more antennas

Corresponding author: M. Krairiksh (kkmonai@kmitl.ac.th).

are placed into the array, significantly degrades MIMO performance [2]. In an environment of limited space, MIMO system can be accomplished by utilizing the independence of the propagation paths of the two different polarizations [3]. Svantesson et al. [4] showed a useful analytical framework for accessing MIMO system, while Dong et al. [5] simulated the channel capacity of MIMO system by exploiting multiple polarizations with a tri-monopole antenna. This kind of antenna offers channel capacity that approaches the capacity of an uncorrelated MIMO Rayleigh channel. Moreover, it was shown that the increase in channel capacity is due mainly to polarization diversity, not pattern diversity. Waldschmidt et al. [6] showed that a system based on the combination of polarization and spatial diversity is best-suited for the situation where a trade-off between space and capacity has to be made. However, mutual coupling exerts tremendous influence on this system which led ultimately to poor performance. Waldschmidt et al. [7] also analyzed the impact of mutual coupling on the capacity of MIMO system with compact antenna array.

In general, antennas for wireless communications are intended either for directional or omnidirectional patterns [8, 9]. Recently, Kosulvit et al. [10] proposed a bidirectional antenna with a probe excited circular ring that is suitable for a long and narrow environment like a corridor or a tunnel. This antenna has a simple design and configuration. The two-probe excited circular ring was used at both ends of MIMO communication system for measuring mutual information. The system performance was significantly improved over those equipped with horizontally-spaced vertical polarized dipole array antennas [11]. In this paper, we incestigate a bidirectional circular ring antenna equipped with two-probe excited ring. To gain insight into the antenna parameters, induced emf method is used in the analysis of radiation characteristics. A transmission line model is utilized to determine the impedance characteristics of the antenna. The antenna design is that the parameters of a single probe antenna are chosen to obtain a suitable ring radius. The parameters of a two-probe antenna that yield suitable probe length and ring length are determined. The design that yields suitable antenna parameters with maximum isolation is identified. Then, isolation between the two probes of the antenna is enhanced by insertion of an inductor coil between them. Finally, a prototype antenna designed to operate at the frequency of 5.2 GHz is fabricated and tested.

2. IMPEDANCE CHARACTERISTICS OF A TWO-PROBE EXCITED CIRCULAR RING ANTENNA

2.1. Input Impedance and VSWR

A two-probe excited circular ring antenna consists of two linear electric probes. The probes have length l and their feeding points are positioned at $(r = a, \theta = \pi/2, \phi = \phi_1')$ and $(r = a, \theta = \pi/2, \phi = \phi_2')$. The probe separation is represented by $\Delta\phi$. They are surrounded by a circular ring antenna with ring radius a and ring length d. The electromagnetic fields propagate from the ring in both z and $-z$ directions. The field radiated from the two apertures at the ends of the ring on the plane $z = -d/2$ and $z = d/2$, as shown in Fig. 1.

The input impedance of the antenna is calculated from the shunt circuit parameters. These parameters are the admittance of the probe and the admittance of the two apertures, neglecting the reflections from the apertures. Precisely, the input impedance of the antenna is the inverse of the total admittance of the equivalent circuit.

Induced emf method is used to calculate the self and mutual impedances of the antennas because it is easy to obtain design parameters from the closed form mathematical expressions [12]. To calculate the self impedance at the feeding probe, sinusoidal current distribution is assumed along the probe length. Under these conditions, the input impedance at the feeding probe (Z_p) can be expressed as

$$Z_p = \frac{j\omega\mu_0}{I_m} \sum_{m=0}^{\infty}\sum_{n=1}^{\infty} \left[\begin{array}{l} c_\zeta m^2 \cos\left[m\left(\phi-\phi'\right)\right] \int\limits_{a-l}^{a} \frac{J_m(\zeta\rho)}{\rho} \sin[k(\rho-a+l)] \\ E_{a,\mathrm{TE}} \left\{ \begin{array}{l} e^{-jk_\zeta(z-z')}; z > z' \\ e^{-jk_\zeta(z'-z)}; z < z' \end{array} \right. d\rho \\ +c_\xi \frac{k_\xi^2}{\kappa_\xi^2} \cos\left[m\left(\phi-\phi'\right)\right] \int\limits_{a-l}^{a} \frac{\partial J_m(\xi\rho)}{\partial\rho} \sin[k(\rho-a+l)] \\ E_{a,\mathrm{TM}} \left\{ \begin{array}{l} e^{-jk_\xi(z-z')}; z > z' \\ e^{-jk_\xi(z'-z)}; z < z' \end{array} \right. d\rho \end{array} \right], \quad (1)$$

where I_m is the maximum current which is equal to unity and $k = \omega\sqrt{\mu\varepsilon}$. ζ and ξ correspond to the transverse electrical mode (TE) and transverse magnetic mode (TM), respectively. They are defined as $\zeta = q_{mn}/a$ and $\xi = p_{mn}/a$ respectively, where q_{mn} and p_{mn} are the eigenvalues for different m and n. These values are tabulated in [13, 14]. J_m is the Bessel function of the first kind of order m. The primed and unprimed coordinates represent the location of source and the observation point, respectively.

The admittance of the probe is equal to the inverse of the input impedance Z_p. The aperture admittance Y_a is calculated as follows

$$
\begin{aligned}
Y_a = & \frac{1}{V^2} \int_0^{2\pi} \int_0^{a} \left[\left[-j\omega\mu_0 \sum_{m=0}^{\infty} \sum_{n=1}^{\infty} \begin{bmatrix} c_\zeta m^2 \frac{J_m(\zeta\rho)}{\rho} \cos\left[m\left(\phi-\phi'\right)\right] \\ E_{a,\mathrm{TE}} \begin{cases} e^{-jk_\zeta(z-z')}; z>z' \\ e^{-jk_\zeta(z'-z)}; z<z' \end{cases} \\ +c_\xi \frac{k_\xi^2}{\kappa_\xi^2} \frac{\partial J_m(\xi\rho)}{\partial\rho} \cos\left[m\left(\phi-\phi'\right)\right] \\ E_{a,\mathrm{TM}} \begin{cases} e^{-jk_\xi(z-z')}; z>z' \\ e^{-jk_\xi(z'-z)}; z<z' \end{cases} \end{bmatrix} \right. \right. \\
& \left. \left. \cdot \sum_{m=0}^{\infty} \sum_{n=1}^{\infty} \begin{bmatrix} c_\zeta \frac{k_\zeta}{\kappa_\zeta} \left(jm^2k\right) \frac{J_m(\zeta\rho)}{\rho} \cos\left[m\left(\phi-\phi'\right)\right] \\ H_{a,\mathrm{TE}} \begin{cases} -e^{-jk_\zeta(z-z')}; z>z' \\ +e^{-jk_\zeta(z'-z)}; z<z' \end{cases} \\ +c_\xi \frac{k_\xi}{\kappa_\xi} \left(jk\right) \frac{\partial J_m(\xi\rho)}{\partial\rho} \cos\left[m\left(\phi-\phi'\right)\right] \\ H_{a,\mathrm{TM}} \begin{cases} -e^{-jk_\xi(z-z')}; z>z' \\ +e^{-jk_\xi(z'-z)}; z<z' \end{cases} \end{bmatrix} \right] \right. \\
& - \left[\left[-j\omega\mu_0 \sum_{m=0}^{\infty} \sum_{n=1}^{\infty} \begin{bmatrix} c_\zeta m \frac{\partial J_m(\zeta\rho)}{\partial\rho} \sin\left[m\left(\phi-\phi'\right)\right] \\ E_{a,\mathrm{TE}} \begin{cases} e^{-jk_\zeta(z-z')}; z>z' \\ e^{-jk_\zeta(z'-z)}; z<z' \end{cases} \\ +c_\xi m \frac{k_\xi^2}{\kappa_\xi^2} \frac{J_m(\xi\rho)}{\rho} \sin\left[m\left(\phi-\phi'\right)\right] \\ E_{a,\mathrm{TM}} \begin{cases} e^{-jk_\xi(z-z')}; z>z' \\ e^{-jk_\xi(z'-z)}; z<z' \end{cases} \end{bmatrix} \right. \right. \\
& \left. \left. \cdot \sum_{m=0}^{\infty} \sum_{n=1}^{\infty} \begin{bmatrix} c_\zeta \frac{k_\zeta}{\kappa_\zeta} \left(jmk\right) \frac{\partial J_m(\zeta\rho)}{\partial\rho} \sin\left[m\left(\phi-\phi'\right)\right] \\ H_{a,\mathrm{TE}} \begin{cases} -e^{-jk_\zeta(z-z')}; z>z' \\ +e^{-jk_\zeta(z'-z)}; z<z' \end{cases} \\ +c_\xi \frac{k_\xi}{\kappa_\xi} \left(jmk\right) \frac{J_m(\xi\rho)}{\rho} \sin\left[m\left(\phi-\phi'\right)\right] \\ H_{a,\mathrm{TM}} \begin{cases} -e^{-jk_\xi(z-z')}; z>z' \\ +e^{-jk_\xi(z'-z)}; z<z' \end{cases} \end{bmatrix} \right] \right] \\
& \cdot \hat{a}_z \rho d\rho d\phi, \qquad (2)
\end{aligned}
$$

where V is the voltage across the aperture. Since the input impedance of the antenna is taken to be the reciprocal of the shunt admittances, the transformation of these admittances at the ends of both apertures (i.e., from $z = \pm d/2$ along the ring length to the probe position $z = 0$) can be accomplished by using the transmission line equation [15]. Finally, the input impedance can be obtained from the inversion of total admittance.

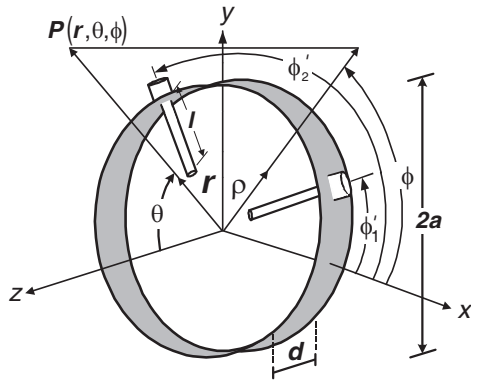

Figure 1. Configuration of the two-probe excited circular ring antenna.

2.2. Mutual Impedance and Isolation

When one antenna is placed near another antenna, its input impedance can be calculated by including the mutual impedance with the self impedance (input impedance without another antenna) and it is called driving point impedance [12]. The mutual impedance (referring to the input current I_{1i} of antenna 1) is

$$Z_{\text{mutual}} = \frac{j\omega\mu_0}{I_m^2 \sin^2(kl)} \sum_{m=0}^{\infty}\sum_{n=1}^{\infty} \left[\begin{array}{l} c_\zeta m^2 \cos\left[m\left(\phi-\phi'\right)\right] \int\limits_{a-l}^{a} \frac{J_m(\zeta\rho)}{\rho} \sin\left[k\left(\rho-a+l\right)\right] \\ E_{a,\text{TE}} \left\{ \begin{array}{l} e^{-jk_\zeta(z-z')} \\ e^{-jk_\zeta(z'-z)} \end{array} \right. d\rho \\ +c_\xi \frac{k_\xi^2}{\kappa_\xi^2} \cos\left[m\left(\phi-\phi'\right)\right] \int\limits_{a-l}^{a} \frac{\partial J_m(\xi\rho)}{\partial\rho} \sin\left[k\left(\rho-a+l\right)\right] \\ E_{a,\text{TM}} \left\{ \begin{array}{l} e^{-jk_\xi(z-z')} \\ e^{-jk_\xi(z'-z)} \end{array} \right. d\rho \end{array} \right] \quad (3)$$

Therefore, the mutual admittance can be calculated from the inverse of the mutual impedance.

Isolation of the antenna can be computed as in [16]. As seen in the expressions of the antenna's input impedance and mutual impedance, it is clear that both of them are dependent on ring radius a, ring length d, probe length l and the angle between the two probes $\Delta\phi$.

3. ANALYSIS OF A TWO-PROBE EXCITED CIRCULAR RING ANTENNA

3.1. One-probe Antenna

Before further investigation, the effect of higher modes on the impedance of the antenna will be examined. So far, we have considered only the dominant mode (TE_{11}) as the propagation mode in the waveguide, but there also exist higher modes affecting the antenna impedance since it is calculated at the feeding probe. The input impedance at the feeding probe of an antenna that has a ring radius of 0.3λ, a ring length of 0.2λ, and a probe length of 0.25λ will be found for the purpose of illustration of the effect of higher modes. Note that the shortest ring length is 0.2λ which is the width of an SMA connector. Since the number of modes is large when the ring length is small, the number of modes obtained from the shortest ring length is used as a representative for those of other ring lengths. Figure 2 shows the summation of impedances from each mn modes with the one from the lower mode. Since resistance is equal to $33.30\,\Omega$ for all cases, only the reactance values are shown in this figure. Because m affects more significant to impedance of the antenna than n, we choose the case $n = 4$ to study the effect of m on the impedance. The differences between the impedances of m and $m + 1$ values, with $n = 4$ modes, are shown in Fig. 2. It is clear that impedance of the antenna does not converge (ΔReactance $\neq 0$) when m and n increase, as can be seen in this figure. The impedance seems to converge at $m = 13$, but ΔReactance increases again at $m = 14$. This kind of fluctuation is observed again as m increases. On the other hand, when we consider

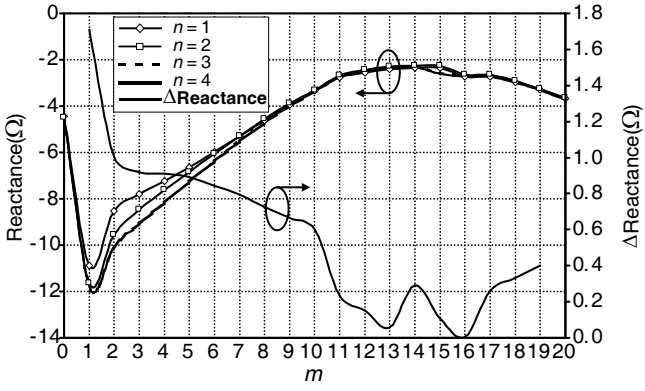

Figure 2. Impedance of the antenna for different m and n values ($a = 0.3\lambda$, $d = 0.2\lambda$, $l = 0.25\lambda$).

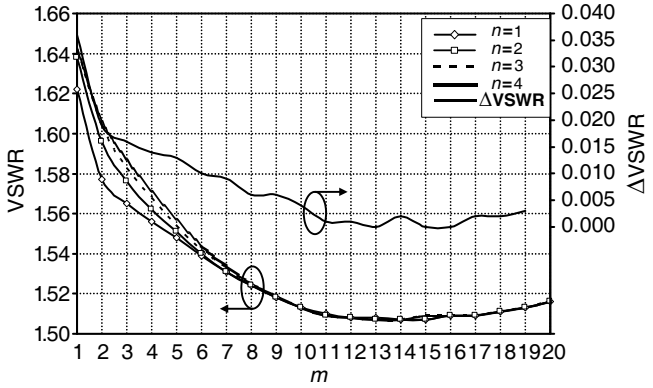

Figure 3. VSWR of the antenna for different m and n values ($a = 0.3\lambda$, $d = 0.2\lambda$, $l = 0.25\lambda$).

the impedance in terms of VSWR, shown in Fig. 3, the fluctuation is not obvious. Note that only the VSWR at the feeding probe is considered and that it starts from $m = 1$ because it is equal to infinity at $m = 0$, where there exists only the reactance term. When only the cases where the variation of VSWR of less than 0.005 is considered, we find the first case when $m = 11$ and $n = 4$ has VSWR of 1.509. The difference between this VSWR and that of $m = 12$ and $n = 4$ is 0.001. Moreover, the differences between the VSWR of any pairs of m and $m + 1$ modes are always lower than 0.005 as m increases beyond 11. Therefore, the values of $m = 11$ and $n = 4$ are chosen in calculations. In addition, we have examined impedance of the TE and TM modes and found that the dominant mode, TE_{11}, has the most significant effect on the impedance of the antenna, and the higher modes, TE_{21}, TM_{11}, TM_{01} and TM_{21}, also shows some influences. However, the results are not enumerated in this paper.

3.2. Two-probe Antenna

In this section, we consider the impedance characteristics of the two-probe excited ring antenna. Both the VSWR of each antenna and the isolation between the two antenna-ports are considered. Since ring length and probe length also have a significant impact on the two-probe antenna performance, their variations are of interest.

To achieve a suitable probe length for a two-probe antenna, VSWR has to be trade-off with isolation. The aim of this study is to achieve the maximum isolation of higher than 20 dB with VSWR of less than 2 : 1.

Fixing the radius at 0.3λ, the angle between the two probes at 90°, and the operating frequency at 5.2 GHz, VSWR and isolation of the antenna are plotted, in Fig. 4, as a function of probe length for various ring lengths. Note that the isolation results are applicable for both the isolation of probe 1 from probe 2 and that of probe 2 from probe 1 since they are identical according to the reciprocity theorem. It is found that the shorter the feeding probe provides the higher the VSWR and isolation. Feeding probe length shorter than 0.23λ yields VSWR higher than 2. Therefore, if isolation higher than 20 dB and VSWR less than 2 are intended for, probe length of 0.25λ is a good choice. Although the probe length of 0.23λ provides 1 dB higher isolation, its

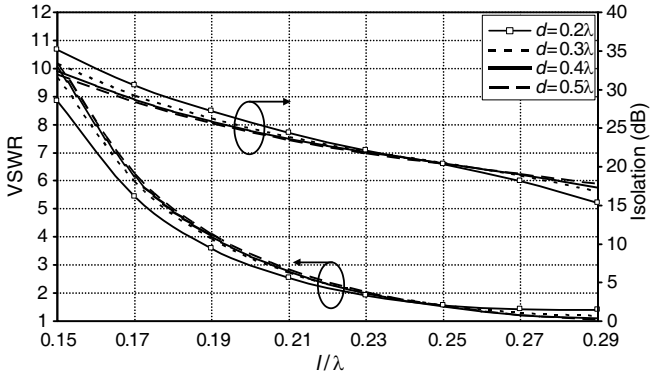

Figure 4. VSWR and isolation of the antenna with varying probe length ($a = 0.3\lambda$, $\Delta\phi = 90°$, $f = 5.2$ GHz).

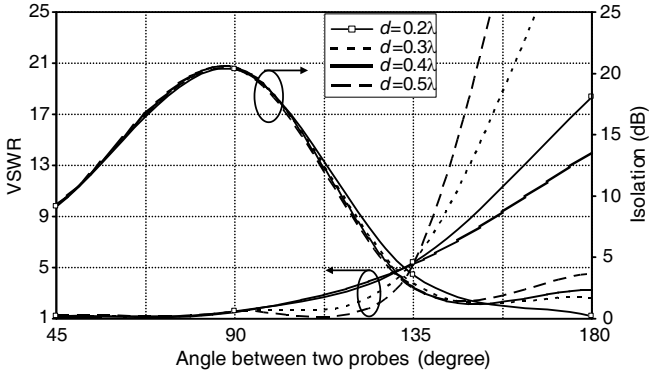

Figure 5. VSWR and isolation of the antenna with varying angle between the two probes ($a = 0.3\lambda$, $l = 0.25\lambda$, $f = 5.2$ GHz).

VSWR is approximately 2 for all ring lengths. Therefore, it is not the best choice. We can see that the variations of VSWR and isolation are in opposite manner. The probe length that achieves desirable VSWR yields undesirable isolation.

Figure 5 shows the VSWR and isolation of the antenna as a function of the angle between the two probes for different ring lengths with probe length fixed at 0.25λ and operating frequency fixed at 5.2 GHz. It is evident that large angle between the two probes provides the high VSWR, while maximum isolation is achieved at the angle of 90° where the two-probe antenna produces orthogonal polarizations. The isolation is higher than 20 dB for all ring lengths at this angle. VSWR increases enormously when the angle between the two probes is larger than 90°. The isolation at these angles is small since the probes produce nearly the same polarization. Finally, high mutual coupling between the two probes was also observed.

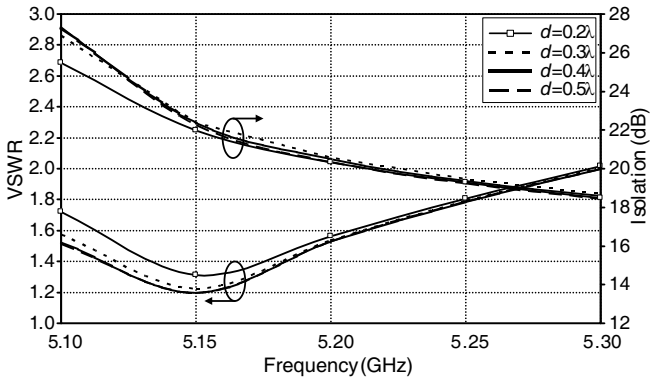

Figure 6. VSWR and isolation of the antenna at various frequencies ($a = 0.3\lambda$, $l = 0.25\lambda$, $\Delta\phi = 90°$).

Table 1. Dimensions of the prototype antenna.

Antenna Parameters	**Physical Dimension at f = 5.2 GHz**
Ring radius (a)	0.3λ (1.73 cm)
Ring length (d)	0.3λ (1.73 cm)
Probe length (l)	0.25λ (1.44 cm)
Angle between two probes ($\Delta\phi$)	90°
Probe diameter	1 mm

Figure 6 shows VSWR and isolation of the antenna as a function of frequency for different ring lengths when the probe length is fixed at 0.25λ and the angle between the two probes is 90°. The frequency range spans from 5.1 GHz to 5.3 GHz. The start frequency is set at 5.1 GHz since the cut-off frequency of this particular ring radius is 5.08 GHz. This frequency range is chosen because it is the operating range of the 5 GHz indoor WLAN, i.e., 5.15–5.25 GHz. The results obtained are as follow: the VSWR of the antenna are less than 2 and the isolation are approximately 20 dB within the operating band for all ring lengths. At the center frequency of 5.2 GHz, ring length of 0.3λ provides maximum isolation. Therefore, we conclude that ring radius of 0.3λ, ring length of 0.3λ, probe length of 0.25λ, and the angle between the two probes of 90° are used to fabricate the prototype antenna. The designed parameters are shown in Table 1. Note that its resonance frequency is not at 5.2 GHz since the probe length that provides maximum isolation is chosen. Table 2 shows the calculated and measured impedances, VSWR, and isolation at 5.2 GHz.

From the mutual impedance in Table 2, the antenna possesses capacitive reactance that originates from mutual interaction between the two probes. To cancel this effect, an air-core inductor coil is inserted between the feeding probes to create a resonance circuit with inductive reactance. This LC series resonance circuit provides high impedance, blocking the current flow from one probe to the other. Since the infinite impedance cannot be created, the isolation between the two probes of the antenna is not infinite. However, the constructed resonance circuit still significantly reduces the current at the end of feeding probes that improves the isolation. In the next section, the measured effect of this inductor coil on VSWR, isolation, and radiation pattern of the antenna will be discussed.

Table 2. Impedance, VSWR, isolation, and gain of the two-probe antenna at the frequency of 5.2 GHz.

Parameters Characteristics	**Without *L***		**With *L***
	Cal.	Meas. ant.1, ant.2	Meas. ant.1, ant.2
Input impedance (Ω)	$32.63 + j4.94$	$57.19 - j21.15$, $33.39 - j14.51$	$85.10 - j21.82$, $33.38 - j20.60$
Mutual impedance (Ω)	$-j6.44$	$8.07 - j24.86$, $6.06 - j25.44$	$6.31 - j5.68$, $6.09 - j5.67$
VSWR	1.54	1.44, 1.43	1.84, 1.88
Isolation (dB)	20.56	11.36, 11.36	22.79, 22.98
Gain (dBi)	4.2	3.94, 3.95	4.23, 4.30

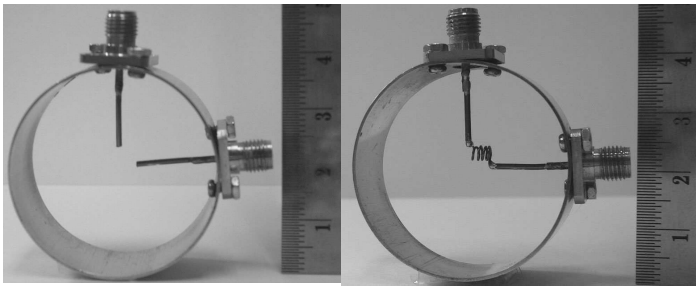

(a) (b)

Figure 7. Photographs of the proposed antenna (a) without an inductor coil (b) with an inductor coil.

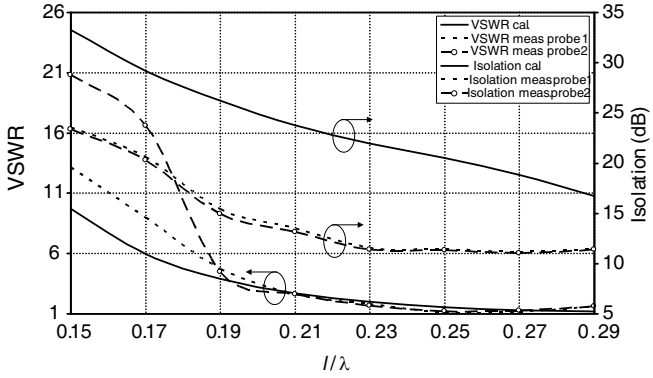

Figure 8. Calculated and measured VSWR and isolation of the antenna with varying probe length ($a = 0.3\lambda$, $\Delta\phi = 90°$, $f = 5.2\,\text{GHz}$).

4. EXPERIMENTAL RESULTS

A prototype antenna was fabricated with the parameters shown in Table 1. Photographs of the antenna without and with inductor coil are shown in Fig. 7. The calculated VSWR and isolation of the antenna without and with inductor coil were compared as functions of probe length with the measured ones. Finally, the radiation patterns and gains of these two antenna configurations were reported.

4.1. Impedance, VSWR and Isolation

VSWR and isolation of the antenna as a function of probe length, obtained from calculation and measurement results, are shown in Fig. 8. The results show good agreement between the calculated

and measured VSWR when probe length is longer than 0.19λ due to the assumed sinusoidal current distribution. However, calculated and measured isolation differed quite significantly. The calculated isolation was 10 dB higher than that of the measured one due to the omission of mutual coupling effect between the two apertures in the calculation. On the other hand, good agreement between calculated and measured VSWR was observed because the impedance of the antenna depended mainly only on probe length, according to [10]. The differences between the calculated and measured VSWR and isolation were 6.5% and 44.7%, respectively, for the probe length of 0.25λ at the fixed frequency of 5.2 GHz. These results exhibited the same trend that ensures that the proposed design principles are reliable.

As seen from the results, the isolation of the fabricated antenna is lower than that of the theoretical one. The same trend can be observed in Table 2 in terms of mutual impedance, i.e., the mutual impedance of the real antenna has a higher capacitive reactance than that of the calculated one. Consequently, a prototype antenna was designed to utilize an inductor coil with higher inductive reactance. A suitable inductor coil was chosen to resonate with the capacitive reactance of the two-probe antenna. The inductance value was approximated by using an expression for an air-core inductor coil reported in [17]. After insertion of the inductor coil, it was clear, as can be seen in Table 2, that the mutual impedance of the antenna was effectively reduced. The capacitive reactance of the antenna was reduced as expected, and enhances the isolation.

Figure 9 shows a comparison between the measured VSWR and isolation of antennas with inductor coil and without inductor coil.

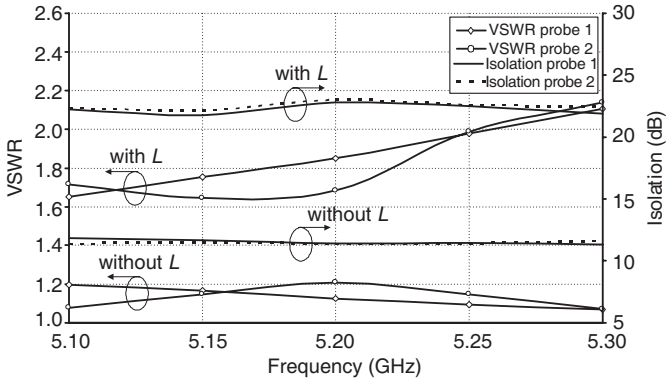

Figure 9. Measured VSWR and isolation of the antennas with and without inductor coil ($a = 0.3\lambda$, $l = 0.25\lambda$, $\Delta\phi = 90°$).

These parameters were shown as functions of frequency. It was obvious that the VSWR of the proposed antenna with inductor coil was higher than that of the proposed antenna without an inductor coil. On the other hand, the isolation of the antenna with inductor coil was 11 dB higher than that of the one without. Since the VSWR of the antenna with to that without the coil was less than 2 : 1, the isolation provided by the coil was higher than 20 dB observed over the desired bandwidth (5.15–5.25 GHz). Choosing the antenna with inductor coil is a good design trade-off.

4.2. Radiation Pattern and Gain

Even after a reasonable trade-off between VSWR and isolation was achieved, the influence of the inserted inductor coil on the radiation pattern of the proposed antenna still had to be investigated. Fig. 10 shows the radiation patterns in the xy-plane of the antenna with and without an inductor coil. It shows that bidirectional radiation patterns were achieved for both of the antenna configurations. When probe 1 was excited and probe 2 was terminated with 50 Ω load, the antenna radiated horizontal polarization as major component and vertical polarization as minor component, as shown in Fig. 10(a) and vice versa as shown in Fig. 10(b). From both figures, the major components of the antenna with and without an inductor coil were the same while their minor components were slightly different. The insertion of inductor coil degraded the cross polarization component of the antenna. Gain of both antennas were approximately 4 dBi in both 0° and 180° directions.

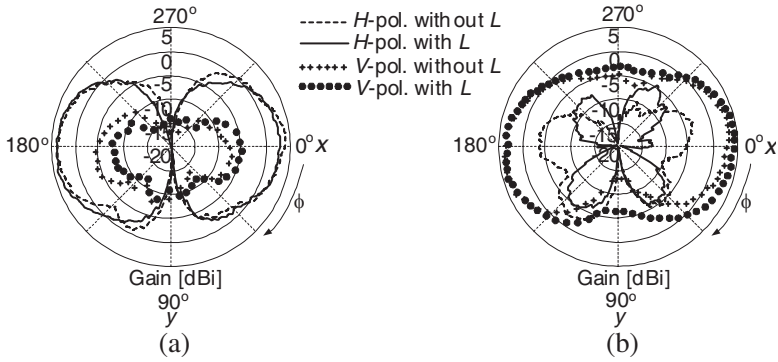

Figure 10. Radiation patterns of the antennas with and without inductor coil (a) Probe 1 is excited and probe 2 is terminated (b) Probe 2 is excited and probe 1 is terminated.

5. DISCUSSION AND CONCLUSION

The performance of the proposed antenna in the MIMO Rayleigh channel was investigated. The angular spectrum of incident waves was assumed to be a Gaussian azimuth spectrum with small angular spread of 5° for both vertical and horizontal polarization, and the main azimuth directions were at 0° and 180°. This angular spectrum represented the expected spectrum in a longitudinally-confined area. The MIMO performance of this antenna was compared to that of the conventional dipole antenna. The results showed that the two-probe excited circular ring antenna with and without inductor coil provided capacities of 7.08 bps/Hz and 6.20 bps/Hz, respectively, which were 1.29 bps/Hz and 0.41 bps/Hz higher than the capacity of a conventional dipole antenna, respectively [11].

To conclude, we proposed a two-probe excited circular ring antenna for a long and narrow environment. Antenna analysis and design were shown in this paper. One salient point is the improvement of isolation between the two probes of the antenna by insertion of an inductor coil. Measurements showed that the isolation achieved was in excess of 20 dB while the VSWR was less than 2 : 1. Bidirectional pattern was satisfactorily accomplished even with the inductor coil installed and the maximum gain was approximately 4 dBi in the desired direction.

ACKNOWLEDGMENT

The work of P. Keowsawat was supported by the Thailand Research Fund (TRF) through the Royal Golden Jubilee Ph.D. Program under Grant no. PHD/0067/2546. The work of M. Krairiksh was supported by the TRF through the Senior Research Scholar Program under Grant No. RTA 5180002.

REFERENCES

1. Sulonen, K., P. Suvikunnas, L. Vuokko, J. Kivinen, and P. Vainikainen, "Comparison of MIMO antenna configurations in picocell and microcell environments," *IEEE J. Sel. Areas Commun.*, Vol. 21, 703–712, Jun. 2003.
2. Jensen, M. A. and J. W. Wallace, "A review of antennas and propagation for MIMO wireless communications," *IEEE Trans. Antennas Propag.*, Vol. 52, 2810–2824, 2004.
3. Kyritsi, P., D. C. Cox, R. A. Valenzuela, and P. W. Wolniansky, "Effect of antenna polarization on the capacity of a multiple element system in an indoor environment," *IEEE J. Sel. Areas Commun.*, Vol. 20, 1227–1239, 2002.

4. Svantesson, T., M. A. Jensen, and J. W. Wallace, "Analysis of electromagnetic field polarizations on multiantenna systems," *IEEE Trans. Wireless Commun.*, Vol. 3, 641–646, 2004.
5. Dong, L., H. Choo, R. W. Heath, Jr., and H. Ling, "Simulation of MIMO channel capacity with antenna polarization diversity," *IEEE Trans. Wireless Commun.*, Vol. 4, 1869–1873, 2005.
6. Waldschmidt, C., S. Schulteis, and W. Wiesbeck, "Complete RF system model for analysis of compact MIMO arrays," *IEEE Trans. Veh. Technol.*, Vol. 53, 579–586, 2004.
7. Waldschmidt, C. and W. Wiesbeck, "Compact wide-band multimode antennas for MIMO and diversity," *IEEE Trans. Antennas Propag.*, Vol. 52, 1963–1969, 2004.
8. Wong, M. T. and C. L. Law, "Influence of microstrip patch antenna heights on wideband channel parameters in a static indoor channel," *International Journal of Electronics*, Vol. 81, 677–698, 1996.
9. Kalis, A., T. Antonakopoulos, C. Soras, and V. Makios, "A switched dual antenna array for mobile computing networks," *International Journal of Electronics*, Vol. 89, 325–335, 2002.
10. Kosulvit, S., M. Krairiksh, C. Phongcharoenpanich, and T. Wakabayashi, "A simple and cost-effective bidirectional antenna using a probe excited circular ring," *IEICE Trans. Electron.*, Vol. E84-C, 443–450, 2001.
11. Keowsawat, P., C. Phongcharoenpanich, S. Kosulvit, J. Takada, and M. Krairiksh, "Mutual information of MIMO system in a corridor environment based on double directional channel measurement," *Journal of Electromagnetic Waves and Applications*, Vol. 23, No. 8–9, 1221–1233, Jun. 2009.
12. Balanis, C. A., *Antenna Theory Analysis and Design*, John Wiley, New York, 1997.
13. Marcuvitz, N., *Waveguide Handbook*, Peter Peregrinus, London, 1986.
14. Balanis, C. A., *Advanced Engineering Electromagnetics*, John Wiley, New York, 1989.
15. Harrington, R. F., *Time-harmonic Electromagnetic Fields*, McGraw-Hill, New York, 1961.
16. Elliott, R. S., *An Introduction to Guided Waves and Microwave Circuits*, Prentice-Hall, Inc., London, 1993.
17. Ludwig, R. and P. Bretchko, *RF Circuit Design*, Upper Saddle River, Prentice-Hall, NJ, 2000.